Energy 261 (2022) 125245

Contents lists available at ScienceDirect

Energy

journal homepage: www.elsevier.com/locate/energy

A simulation model for the design and analysis of district systems with simultaneous heating and cooling demands

Marwan Abugabbara *, Saqib Javed, Dennis Johansson

Department of Building and Environmental Technology, Division of Building Services, Lund University, 221 00 Lund, Sweden

ARTICLE INFO

Keywords:
District heating and cooling
5GDHC
Decentralised substations
Heat pumps
Modelica

ABSTRACT

Latest generations of district heating and cooling systems are characterised by low network temperature with uninsulated pipes, decentralised heat pumps and chillers to modulate the network temperature, and shared energy flows between interconnected buildings. This paper presents a simulation model for the design and analysis of these systems. The model was developed using the Modelica language and it consists of component models from thermal, fluid, and control domains. The model was employed to simulate and analyse the first existing Swedish district system with simultaneous heating and cooling demands and bidirectional energy flows. The system currently connects nine buildings with total respective annual heating and cooling demands of 4.2 and 1.2 GWh. Simulation results revealed several benefits for integrating district and heat pump technologies, including (1) sharing energy flows between interconnected buildings to cover 40 % of the total carried heat in the network, (2) reducing the total purchased energy by 69 % compared to a traditional four-pipe district system, and (3) reducing distribution losses by 28 % compared to traditional networks with insulated pipes. The model can be utilised to support future research and development of new advanced district heating and cooling systems.

1. Introduction

Heating and cooling demands in existing and future buildings will vary due to climate change, urbanisation, and the global increase of living standards [1,2]. The International Energy Agency has projected that space cooling demands will be tripled between 2016 and 2050 and that two-thirds of the world's households could potentially install systems for comfort cooling [3]. At the same time, the demands for heating will still exist for domestic hot water production and space heating. Therefore, the need for integrated heating and cooling systems becomes increasingly important.

The integration between district heating and cooling (DHC) and heat pump technologies is an effective solution that can offer several benefits, including, for example, (1) efficient decarbonisation of the building sector, (2) high and reliable security of supply to connected buildings, (3) lower risks for fire and gas explosions in buildings since individual heating and cooling systems with hazardous fuels are eliminated, and (4) increased community resilience by connecting buildings suffering from energy poverty to a district system [4–7].

District heating (DH) and heat pumps are the two largest heat sources that supply heat to Swedish residential and public buildings. The market share for DH in 2014 was about 55%, whereas heat pumps had 25% of the market share [8]. Sweden has also a large district cooling (DC) market that delivered about 1 TWh in 2019 for both comfort and process cooling applications [9]. These figures indicate potential for leading the heating and cooling markets by leveraging the benefits of DHC and heat pump technologies.

1.1. Development of district heating and cooling

District heating networks have evolved through four generations that were categorised and defined by Lund et al. [10]. The first generation was introduced in Lockport in the United States in the late 19th century and used steam as a heat carrier [11]. Since steam systems had a high risk of explosion, the steam was replaced by pressurised water with high temperatures in the second generation. In the 1980s, building space heating was typically provided by radiators with a supply temperature of around 80 °C. This led to the development of the third generation which is commonly referred to as Scandinavian district heating since many of its components were prefabricated in Scandinavian countries [12]. Although the third generation is widely spread, a large share of the input heat is lost through the distribution pipes due to the high network temperature. The fourth generation addressed this issue by lowering the network temperature to around

* Correspondence to: Faculty of Engineering, Lund University, Box 118, 221 00 Lund, Sweden.
E-mail address: marwan.abugabbara@hvac.lth.se (M. Abugabbara).

https://doi.org/10.1016/j.energy.2022.125245
Received 24 June 2022; Received in revised form 19 August 2022; Accepted 20 August 2022
Available online 28 August 2022

Nomenclature

Abbreviations

5GDHC	Fifth-Generation District Heating and Cooling
ASHP	Air-Source Heat Pump
BU	Balancing Unit
CDF	Cumulative Distribution Function
DC	District Cooling
DH	District Heating
DHC	District Heating and Cooling
DSS	Decentralised Substation
FSM	Finite State Machine

Latin letters

c_p	Specific heat capacity [J/kg K]
K_2	Constant for computing pipe pressure drops
$\dot{Q}$	Heat flow rate [W]
$\dot{V}$	Volume flow rate [m^3/s]
$\dot{m}$	Mass flow rate [kg/s]
A	Amplitude
L	Pipe segment length [m]
B	Pipe burial depth [m]
C	Horizontal distance between centre of pipes [m]
D	Pipe outer diameter [m]
F	Factor for accounting pressure loss in pipe fittings
P	Power [W]
R	Thermal resistance [K/W]
Re	Reynolds number
T	Temperature [K]
Z	Absolute error [%]
d	Pipe inner diameter [m]
e	Pipe relative roughness [m]
k	Fixed flow resistance factor at nominal flow
y	Control signal

Greek letters

ΔT	Temperature difference [K]
Δp	Pressure drop [Pa]
α	Thermal diffusivity [m^2/s]
β	Dimensionless resistance parameter
γ	Modified pipe wall friction factor
ε	Heat exchanger effectiveness
η	Efficiency
λ	Thermal conductivity [W/m K]
μ	Fluid dynamic viscosity (Pa s)
ρ	Fluid density [kg/m^3]
τ	Annual period length [s]

Subscripts

a	Anti-symmetrical
c	Cooling/cold
CH	Chiller
$comp$	Compressor
$cond$	Condenser
dis	District
$evap$	Evaporator
h	Heating
HP	Heat Pump
hx	Heat exchanger
hyd	Hydraulic
lea	Leaving
mea	Measured
mod	Modelled
mot	Motor
ms	Mean surface
nom	Nominal
pri	Primary
ret	Return
s	Symmetrical
sec	Secondary
set	Setpoint
sup	Supply
ug	Undisturbed ground
w	Warm

40 °C, which allowed the integration of low-enthalpy renewable energy sources such as solar and geothermal [10].

In a recently published paper, Østergaard et al. [13] have categorised similar four generations for DC systems. The first generation was introduced in the USA in the late 19th century as a pipeline refrigeration system to supply cooling to the food industry. The second generation was introduced in the 1960s to provide comfort cooling to commercial and public buildings by using large compression or absorption chillers with cold water as the distribution fluid. A third generation emerged in the 1990s to utilise diversified and decentralised cold sources as well as heat recovery from compression chillers and short-term cold storage. The future fourth generation is based on the synergy with other energy sectors such as the electricity and heating sectors. Several technologies such as electric heat pumps, absorption heat pumps, ambient sources, and cold storage are integrated into a smart energy system based on renewable energy sources.

During the latest few years, fifth-generation district heating and cooling (5GDHC) has been developed. It is characterised by additional reduction in the network temperature as well as the ability to supply simultaneous heating and cooling. A typical 5GDHC network operates at temperature levels close to the ambient temperature (<40 °C). Therefore, installing decentralised heat pumps and/or mechanical chillers is necessary to adjust the network temperature to the desired building supply temperatures. Such operating principle allows combining heating and cooling where energy can be shared between connected prosumers who produce/consume energy towards/from the network. Consequently, the potential for waste-heat recovery is increased and the energy efficiency of the district network is improved. Since the 5GDHC is a fairly new complex district heating and cooling concept, there is a lack of a common vocabulary as different names can be found in the literature [14,15]. These include, e.g., *fifth-generation district heating and cooling* [16–19], *ultra-low networks* [20–22], and *bidirectional networks* [23,24], among others.

Buffa et al. [25] reviewed existing 5GDHC systems in Europe. The current status and development of 5GDHC is reported by Jonas et al. [17]. Wirtz et al. [26] presented an optimisation approach for designing 5GDHC systems using mixed-integer linear programming. A topology analysis tool was developed by von Rhein et al. [27] using the Modelica language [28] to determine the most feasible way to connect prosumers to either existing or new 5GDHC networks. Sommer et al. [29] also used Modelica to compare a single-pipe 5GDHC network (referred to as the reservoir network) to a double-pipe 5GDHC network.

Millar et al. [30] generated demand profiles for several buildings with rarely occurring simultaneous heating and cooling and highlighted the need for energy storage to utilise the shared energy for later usage. Meibodi and Loveridge [31] evaluated the possible integration between energy geostructures (e.g., energy walls, energy piles, and energy tunnels) and 5GDHC systems.

Based on the literature, it can be noticed that previous research has investigated particular aspects of 5GDHC systems such as component sizing and network topology analysis. However, there is still a need to investigate these new advanced systems from a global perspective combining several technical aspects. Our research attempts to bridge this gap by presenting a simulation model for the design and analysis of 5GDHC systems including thermo-fluid and control components. To the authors' best knowledge, no previous work has investigated 5GDHC systems using a multi-domain approach with an analysis of network heat losses in uninsulated pipes. The model can therefore support the planning and analysis of new advanced DHC concepts.

1.2. Modelling of advanced district heating and cooling concepts

The literature review has shown that 5GDHC systems may incorporate several design options, such as the choice of network topology and the type of energy source. This poses challenges to model and analyse changes in the system which are expected to take place during the initial design stage or operation as well as future network expansion. Therefore, methods that support multi-domain modelling and provide flexibility in adapting changes in the model architecture are necessary. Modelica is regarded by the International Energy Agency as one of the new generation computational tools for modelling building and community energy systems [32]. It is also recommended by researchers, including Abugabbara et al. [33], for modelling 5GDHC systems.

Modelica is a free and open-source equation-based objected-oriented modelling language that supports multi-domain modelling of complex physical systems. The behaviour of physical systems is described using differential–algebraic and discrete equations that are encapsulated inside an icon that represents the model [34]. To build models of large physical systems, smaller component models are connected through connection lines that exchange model variables through standardised interfaces. Therefore, there is no need for an explicit definition of input/output relationships between the models. Instead, the variables are computed by efficient solvers as long as the boundary conditions at the connection ports are sufficient to solve the system of equations.

Robust Modelica models for building and energy systems are available for free in several libraries, such as the Modelica *Buildings* library [35] developed at Lawrence Berkeley National Laboratories in the USA, *AixLib* [36] from RWTH Aachen in Germany, and *IDEAS* [37] from KU Leuven in Belgium. Component models from existing libraries can be used either directly or after customising them to suit the need of the end-user. Researchers and end-users alike can therefore utilise the available component models to develop a simulation model for advanced district systems such as 5GDHC systems.

1.3. Paper aims, contribution, and organisation

The aim of this paper is to present the development of a simulation model for the design and analysis of 5GDHC systems with two-pipe network topology and bidirectional energy flows, including main thermo-fluid components and control strategies. Additionally, the paper aims to present the potential and anticipated system performance under semi-ideal conditions. The paper contributes to the growing area of research on new and advanced district heating and cooling technologies by presenting and utilising the simulation model to analyse the first existing Swedish 5GDHC system. Additionally, the model can be utilised to monitor an existing 5GDHC system, analyse network losses in uninsulated distribution pipes, and forecast heat injection/extraction into/from the network. The study findings could be used to explore future possibilities for a wider implementation of 5GDHC systems.

The development of the simulation model is firstly described in Section 2 following a gradual progression from modelling small components up to modelling the entire district system. Annual simulation results are then presented in Section 3 for an in-depth analysis of the system operation. This is followed by Section 4 discussing the main findings and practical recommendations for wider implementation of 5GDHC systems. Finally, conclusions and future work are outlined in Section 5.

2. Methods and material

This section provides a classification of the system components used in the simulation model. Next, the Modelica implementation of thermo-fluid components and control strategies is described. A 5GDHC network is then assembled using the system components. Finally, the model validation and limitations, and the system performance indicators are clarified.

2.1. System description

The description of a 5GDHC system at different levels of abstraction is illustrated in Fig. 1. The illustration can also be seen as a modelling hierarchy that supports dividing the large district system into smaller subsystems and further down to single components. At the highest level of abstraction, the district system connects prosumers through a ring network with two pipes denoted as warm and cold pipes. A balancing unit is responsible for injecting or rejecting heat into/from the network depending on the dominant demand type and the temperature levels in the network. This function is primarily achieved by a reversible air-source heat pump. In the heat rejection mode, a cooling tower is also realised. Another important function of the balancing unit is to pressurise the network such that it ensures sufficient delivery of flow. Thus, an accumulator tank is incorporated to provide a desired static pressure. The magnified part in Fig. 1 shows the main components in a prosumer's decentralised substation designed for simultaneous heating and cooling demands, and includes a heat pump, a chiller, and a free-cooling heat exchanger. In the subsystem level, the system is divided into three independent subsystems that can be modelled and tested separately. Finally, individual components are described by differential–algebraic equations using Modelica syntax. Components for building and energy systems are modelled by reusing or editing existing components from finished Modelica libraries. Components from the Modelica *Buildings* libraries version 8.1.0 were used in this study and the model for the district system was assembled following a bottom-up approach.

2.2. Models for thermo-fluid components

This section presents models for the main subsystems that constitute a 5GDHC network, i.e., decentralised substations, distribution pipes, and the balancing unit.

2.2.1. Model for decentralised substations

A decentralised substation (DSS) can serve an individual building or multiple buildings at the same time. The type of technical installations in any DSS depends on the building demand type. Fig. 2 shows a Modelica diagram view of the main components included in a typical DSS with both heating and cooling demands. The figure is assisted with number labels that are used to explain the model behaviour at different points. Data for heating and cooling demands, and supply temperatures are first prescribed at point 01. The heating and cooling mode controllers are placed at points 02 and 03, respectively. The building heating return temperature $T_{ret,h}$ is expressed at point 04 as:

$$T_{ret,h} = T_{sup,h} - \Delta T_{HP,cond} \quad (1)$$

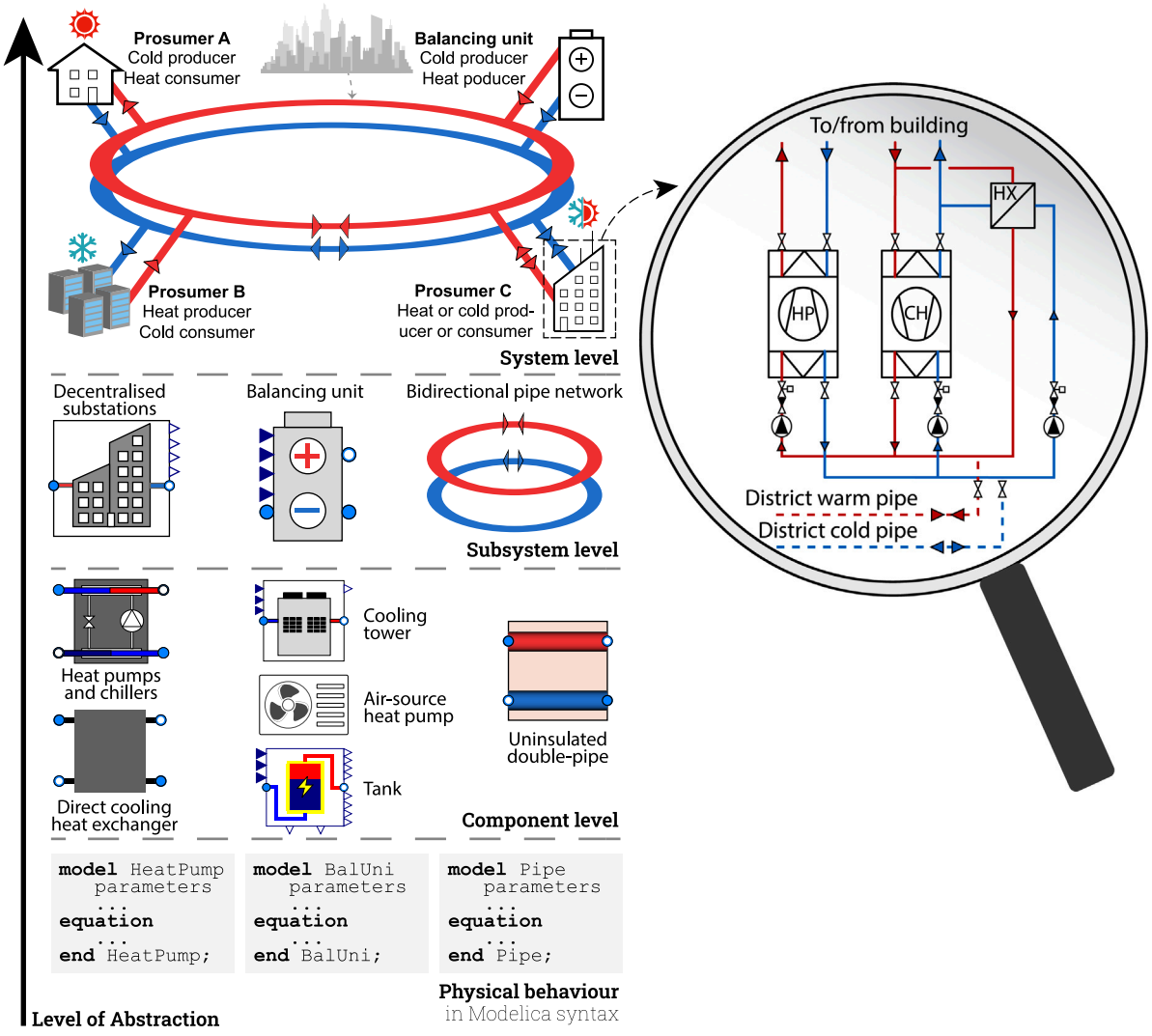

Fig. 1. Different levels of abstraction for a 5GDHC system.

where $T_{sup,h}$ is the heating supply temperature, and $\Delta T_{HP,cond}$ is the temperature difference between the heat pump condenser inlet and outlet. The circulation pump at point 05 draws water to the inlet of the heat pump condenser in the amount of:

$$\dot{m}_{HP,cond} = \frac{\dot{Q}_h}{\Delta T_{HP,cond} \cdot c_{p,water}} \cdot y_h \tag{2}$$

where $\dot{Q}_h$ is the heat demand, $c_{p,water}$ is the specific heat capacity of water, and y_h is the heating mode control signal that determines the pump's state of operation. The required heating supply temperature defined at point 06 is equivalent to the heat pump condenser leaving temperature $T_{HP,cond}$, and the heat pump model shown at point 07 computes the coefficient of performance (COP) based on a prescribed Carnot efficiency η_{Carnot} as:

$$COP_{HP} = \eta_{Carnot} \cdot \frac{T_{HP,cond}}{T_{HP,cond} - T_{HP,evap}} = \frac{\dot{Q}_h}{P_{comp}} \tag{3}$$

where $T_{HP,evap}$ is the temperature of the heat pump evaporator, and P_{comp} is the compressor electric power. The building heating loop is then closed by including the heat sink shown at point 08. The heat pump delivered thermal power and the total electric power used by the compressor and the circulation pumps are marked at point 09 and 10, where the electric power of the circulation pump P_{pump} is defined as:

$$P_{pump} = \frac{\dot{V} \cdot \Delta p}{\eta_{hyd} \cdot \eta_{mot}} \tag{4}$$

where $\dot{V}$ is the volume flow rate, Δp is the pump pressure rise, and η_{hyd} and η_{mot} are respectively the hydraulic and motor efficiencies.

At the heat pump source side, two loops can be found to establish hydraulic separation between the building demand side and the district supply side for safe operation. Moreover, the heat pump evaporator may need to operate at a temperature difference and a flow rate different from that in the district loop to avoid freezing. As such, the mass flow entering the heat pump evaporator at point 11 equals to:

$$\dot{m}_{HP,evap} = \frac{\dot{Q}_h - P_{comp}}{\Delta T_{HP,evap} \cdot c_{p,water}} \cdot y_h \tag{5}$$

A similar procedure takes place when cooling demands exist. Unlike the heating mode where only the heat pump delivers all heating demand, cooling can be delivered either by the chiller or the free-cooling heat exchanger or a combination of both. The explanation provided below assumes that both the chiller and the free-cooling heat exchanger operate at the same time. In such mode, the chiller provides the amount of cooling that exceeds the capacity of the free-cooling heat exchanger. The return temperature from the building cooling loop $T_{ret,c}$ is described at point 13 as:

$$T_{ret,c} = T_{sup,c} - \Delta T_{CH,evap} \tag{6}$$

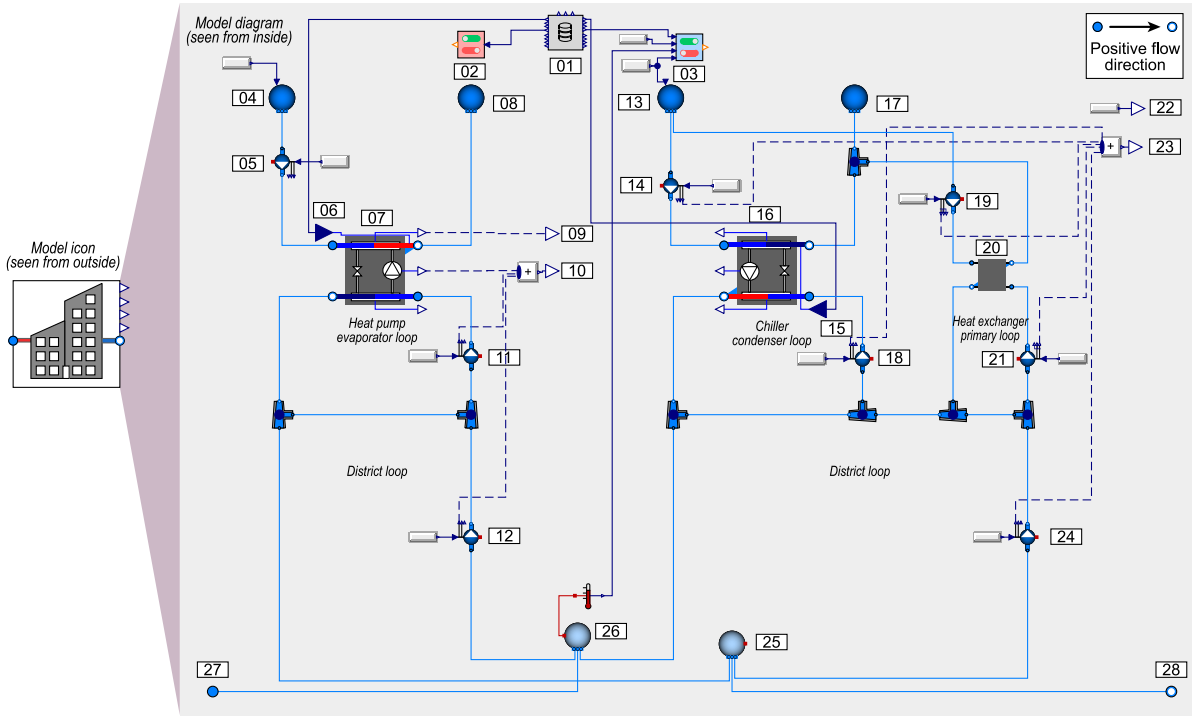

Fig. 2. Diagram view of a decentralised substation with heating and cooling demands. The diagram is assisted with number labels that correspond to the model description provided in Section 2.2.1.

where $T_{sup,c}$ is the cooling supply temperature, and $\Delta T_{CH,evap}$ is the temperature difference between the chiller evaporator inlet and outlet. The circulation pump at point 14 draws water to the inlet of the evaporator equivalent to:

$$\dot{m}_{CH,evap} = \frac{\dot{Q}_c - \dot{Q}_{hx}}{\Delta T_{CH,evap} \cdot c_{p,water}} \cdot y_c \tag{7}$$

where $\dot{Q}_c$ is the cooling demand, $\dot{Q}_{hx}$ is the heat transfer rate of the free-cooling heat exchanger, y_c is the cooling mode control signal that activates the corresponding circulation pumps.

The leaving temperature of the chiller's evaporator is prescribed at point 15 and the COP of the chiller shown at point 16 is determined as:

$$COP_{CH} = \eta_{Carnot} \cdot \frac{T_{CH,evap}}{T_{CH,cond} - T_{CH,evap}} = \frac{\dot{Q}_c}{P_{comp}} \tag{8}$$

The cold water is then supplied to the building cold sink marked at point 17. The circulation pump at point 18 draws water from the district loop to the warm side of the chiller as:

$$\dot{m}_{CH,cond} = \frac{\dot{Q}_{CH,cond}}{\Delta T_{CH,cond} \cdot c_{p,water}} \cdot y_c \tag{9}$$

Similarly, the pumps at the secondary and primary sides of the free-cooling heat exchangers marked respectively at points 19 and 21 draw:

$$\dot{m}_{hx} = \frac{\dot{Q}_c}{\Delta T_{hx} \cdot c_{p,water}} \cdot y_c \tag{10}$$

The corresponding heat transfer rate of the free-cooling heat exchanger becomes:

$$\dot{Q}_{hx} = \varepsilon \cdot \dot{m}_{hx} \cdot c_{p,water} \cdot (T_{pri,in} - T_{sec,in}) \tag{11}$$

where ε is the heat exchanger effectiveness that is computed based on the number of transfer units, the ratio between minimum to maximum flow rate, and the flow regime; $T_{pri,in}$ is the inlet temperature at the primary side; and $T_{sec,in}$ is the inlet temperature at the secondary side. Finally, the delivered cooling power and the corresponding electric power are expressed at points 22 and 23, respectively.

Energy is shared locally inside the decentralised substation at the fluid volumes shown at points 25 and 26. At times when the DSS has dominant heating demands, it extracts water from the warm district pipe connected to the fluid port depicted at point 27. On the contrary, the DSS extracts water from the cold district pipe at point 28 when cooling dominates.

2.2.2. Model for distribution pipes

The model for distribution pipes is divided into two parts based on thermal and hydraulic aspects. The pipes are discretised into n segments along the flow path. For each segment, the thermal part is described using steady-state heat losses that are calculated according to Standard SS-EN 13941-1 [38] and adapted for uninsulated pipes. The calculation is based on the multipole method originally described in [39]. In such a method, heat losses are calculated based on a superposition of a symmetrical problem (interaction between pipes and surroundings and not with each other) and an anti-symmetrical problem (interaction between pipes and not with the surroundings). Fig. 3(a) illustrates the problem, and the equivalent resistance model adopted from van der Heijde et al. [40] is shown in Fig. 3(b). The Modelica implementation is then shown in Fig. 3(c).

The zero-order multipole formulae for the symmetrical resistance R_s is expressed as:

$$R_s = \frac{1}{2 \cdot \pi \cdot \lambda_{soil}} \cdot \left[ln\left(\frac{4 \cdot H_o}{D}\right) + \beta + ln\left(\sqrt{1 + \left(\frac{2 \cdot H_o}{C}\right)^2}\right)\right] \tag{12}$$

where λ_{soil} is the soil thermal conductivity, H_o is a corrected depth taking into account the ground surface resistance as $H_o = H + R_o \cdot \lambda_{soil}$, D is the pipe outer diameter, β is a dimensionless resistance parameter equivalent to:

$$\beta = \frac{\lambda_{soil}}{\lambda_{pipe}} \cdot ln\left(\frac{D}{d}\right) \tag{13}$$

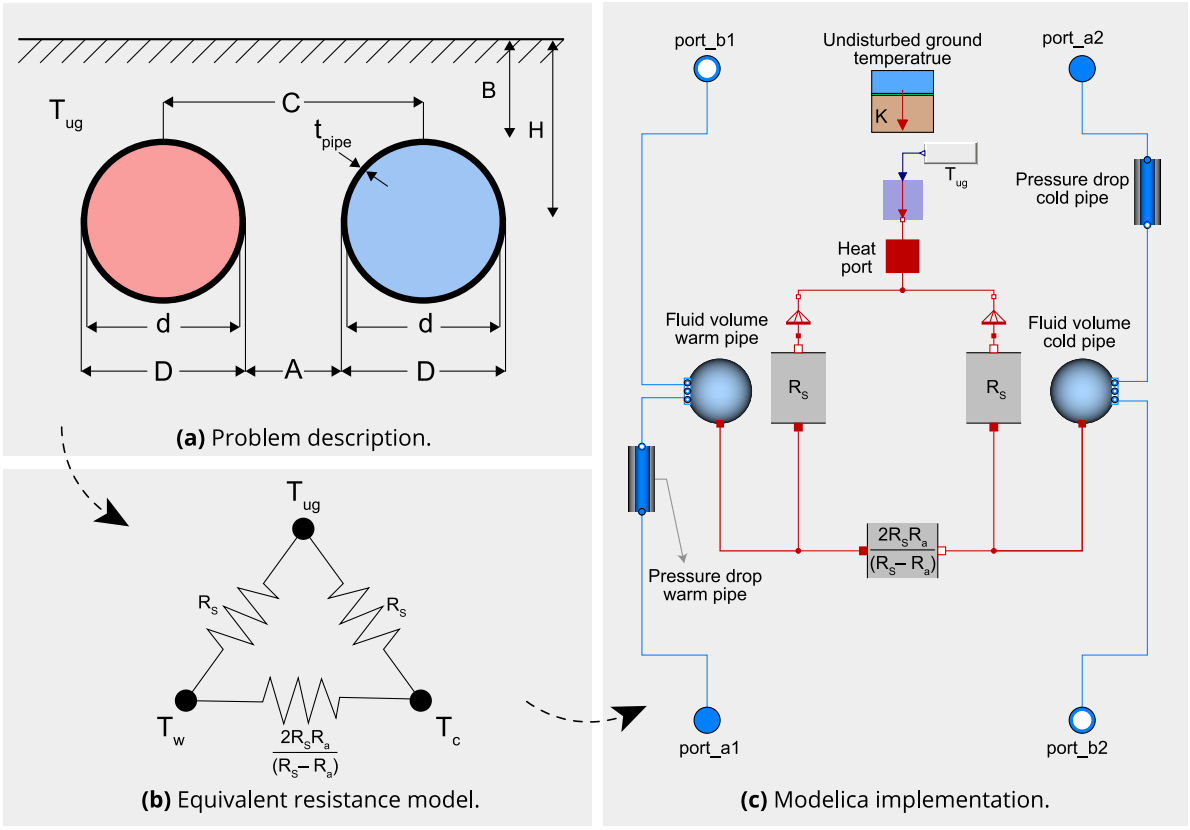

Fig. 3. Description of a steady-state heat loss problem in a double buried pipe. The Modelica implementation is presented for one discretisation element along the pipe path.

where λ_{pipe} is the pipe material thermal conductivity and d is the pipe inner diameter. On the other hand, the anti-symmetrical resistance R_a is expressed as:

$$R_a = \frac{1}{2 \cdot \pi \cdot \lambda_s} \cdot \left[ln\left(\frac{4 \cdot H_o}{D}\right) + \beta - ln\left(\sqrt{1 + \left(\frac{2 \cdot H_o}{C}\right)^2}\right)\right] \tag{14}$$

Once the resistances are defined, the temperatures of the warm and cold fluids are simulated dynamically and interfaced with the resistances at the heat ports denoted in red squares in Fig. 3(c). Finally, the undisturbed ground temperature at the pipe burial depth B is described based on site weather parameters and according to the following formula presented in the ASHRAE District Heating guide [41]:

$$T_{ug,B} = T_{ms} + A_s e^{-B\sqrt{\frac{\pi}{\alpha \cdot \tau}}} sin\left(\frac{2\pi\,(t - t_{lag})}{\tau} - B\sqrt{\frac{\pi}{\alpha \cdot \tau}}\right) \tag{15}$$

where T_{ms} is the site mean annual surface temperature, A_s is the surface temperature amplitude, B is depth, α is the soil thermal diffusivity, τ is the annual period length, t is the calculation timestep, and t_{lag} is the phase lag of the soil temperature.

Heat losses (or heat gains) in each segment of the warm pipe can now be expressed as the arithmetic sum of the symmetrical and anti-symmetrical components as:

$$\dot{Q}_{loss/gain,w} = \left[\frac{1}{R_s} \cdot (T_w - T_{ug}) + \frac{R_s - R_a}{2 \cdot R_s \cdot R_a} \cdot (T_w - T_c)\right] \tag{16}$$

where T_w is the warm fluid temperature, T_c is the cold fluid temperature, and T_{ug} is the undisturbed ground temperature. Likewise, heat losses in the cold pipe are described as:

$$\dot{Q}_{loss/gain,c} = \left[\frac{1}{R_s} \cdot (T_c - T_{ug}) + \frac{R_s - R_a}{2 \cdot R_s \cdot R_a} \cdot (T_c - T_w)\right] \tag{17}$$

In the expressions provided in Eqs. (16) and (17), a negative sign indicates heat gains.

As for the second part of the distribution pipes model, the pipe pressure drop is calculated based on the following relationship between the mass flow rate and the pressure drop:

$$\dot{m} = k \cdot \sqrt{\Delta p} \tag{18}$$

where k is a fixed flow resistance that depends on nominal design parameters. The nominal pressure drop in each pipe segment is expressed as:

$$\Delta p_{nom} = F \cdot K_2 \cdot \gamma(Re, e) \tag{19}$$

where F is a factor that includes the pressure losses of the pipe fittings, K_2 is a constant that takes into account the pipe geometry and the fluid properties, and γ is a modified pipe wall friction factor that depends on Reynolds number Re and the pipe relative roughness e. The constant K_2 is equivalent to:

$$K_2 = \frac{L \cdot \mu^2}{2 \cdot d^3 \cdot \rho} \tag{20}$$

where L is the length of one pipe segment, μ is the fluid dynamic viscosity, d is the pipe inner diameter, and ρ is the fluid density.

The modified friction factor γ is intended for a robust numerical description of the pipe wall friction factor to avoid divisions by zero. A detailed description of the approach followed in Modelica to compute the modified friction factor can be found in the online documentation available in Ref. [42].

2.2.3. Model for system balancing unit

Fig. 4 shows Modelica diagram views of the component models included in the balancing unit (BU) at different levels of abstraction. The reference static pressure is described in the middle diagram at *port_a1*. The cold and warm district pipes are connected to *port_a* and *port_b*, respectively. The BU includes three main components, i.e., a reversible air-source heat pump (ASHP), an accumulator tank, and

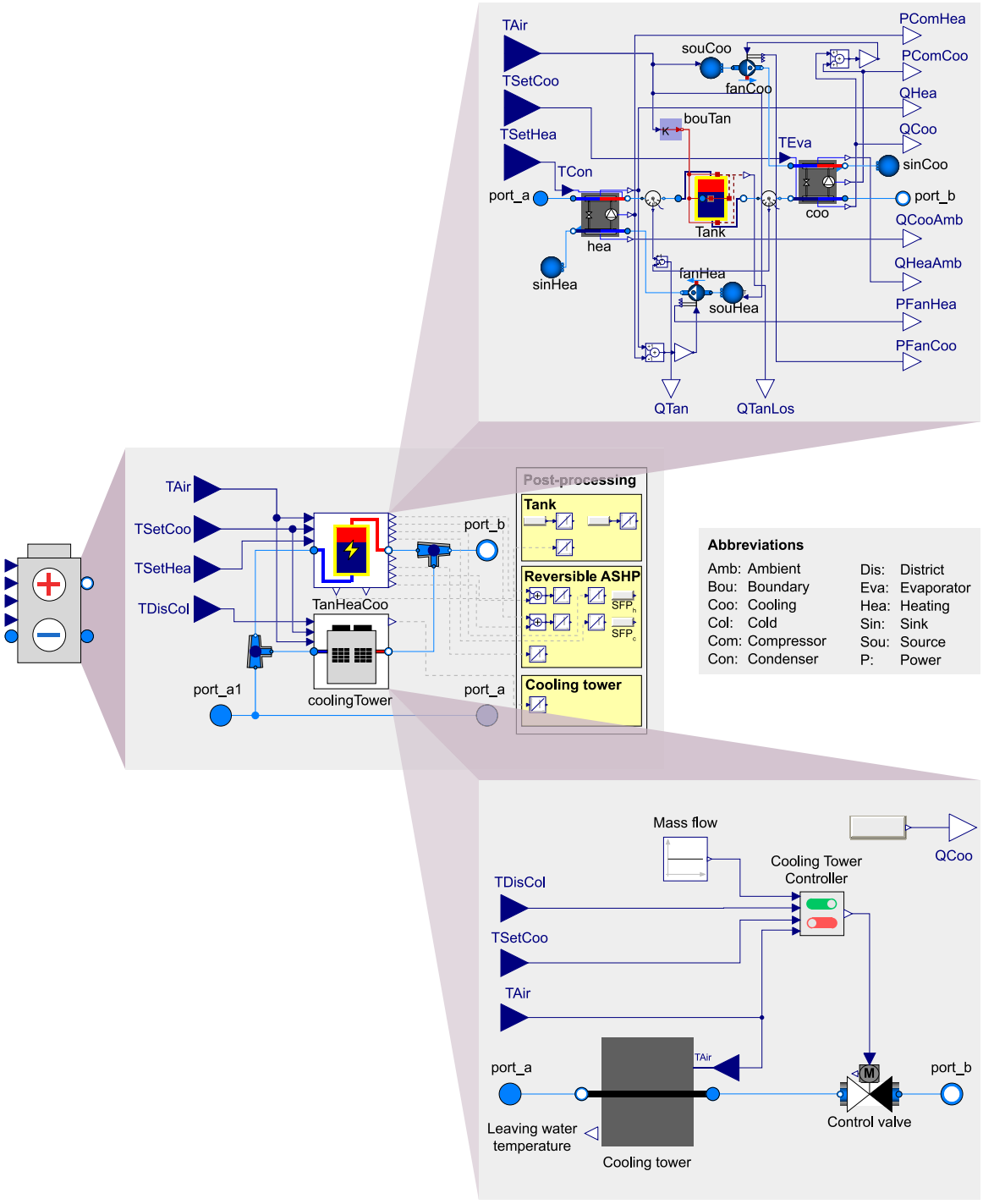

Fig. 4. Diagram view of a balancing unit which includes reversible air-source heat pump, accumulator tank, and cooling tower. Blue arrows denote input control signals, while white arrows interface output variables for post-processing.

a cooling tower. The ASHP and the tank are configured such that the ASHP maintains the temperature in the tank within the network temperature setpoints. The district network is a closed system and, therefore, the total mass flow (after local energy sharing inside the DSS) circulates through the balancing unit.

In the heating mode, the balancing unit activates the ASHP to ensure that the temperature of the warm pipe does not fall below a prescribed heating setpoint. Similarly, the balancing unit controls the temperature of the cold pipe such that it does not exceed a prescribed cooling setpoint. Priority in the cooling mode is given to the cooling tower over the ASHP as long as the operating conditions of the cooling tower are satisfied. The cooling tower is modelled with a constant approach temperature ΔT_{APP} as:

$$\Delta T_{APP} = T_{water,lea} - T_{air,in} \tag{21}$$

where $T_{water,lea}$ is the temperature of the leaving cold water, and $T_{air,in}$ is the air inlet temperature. The heat removed from the water by the cooling tower $\dot{Q}_{coo,tower}$ is equivalent to:

$$\dot{Q}_{coo,tower} = \dot{m} \cdot c_{p,water} \cdot \left(T_{water,lea} - T_{dis,w}\right) \tag{22}$$

where $T_{dis,w}$ is the temperature of the warm district pipe. The reversible ASHP is activated in a cooling mode when the cooling tower is not in

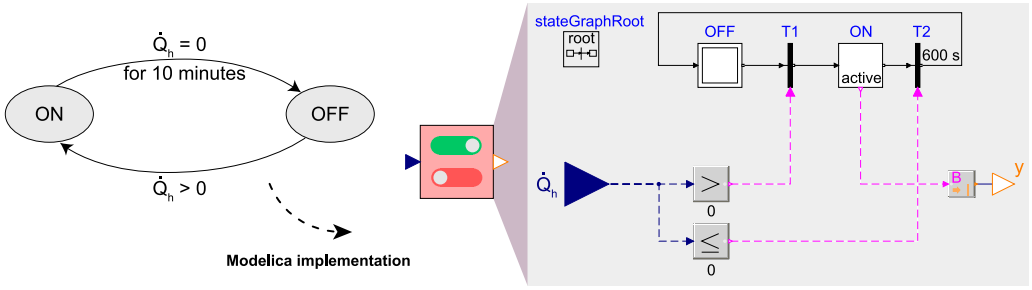

Fig. 5. State graph for the heating mode controller (left) and equivalent Modelica implementation (right).

operation or when additional cooling power is required. From the fluid ports shown in the model icon of the balancing unit, one can interpret the flow direction. For instance, the flow direction from *port_a* to *port_b* indicates dominant heating demands with heat injection into the network, while a flow direction from *port_b* to *port_a* denotes dominant cooling demands with heat rejection from the network.

2.3. Control strategies for component and system operation

This section defines the logics behind controlling the different system components and the entire district system.

2.3.1. Control of decentralised substations

Heating and cooling equipment in DSS are controlled using the finite state machine (FSM) algorithm. This kind of algorithm is convenient for modelling discrete events and reactive systems where the controlled equipment is decomposed into different modes of operation, i.e., states. The controlled equipment is allowed to be only in one state at a time, and the transition between the different states is determined by the controller based on a set of logical conditions [43]. FSM has been previously used by many researchers to control building and energy systems. Fu et al. [44] implemented an FSM algorithm to control a chiller in a data centre. Another FSM control logic was developed by Hinkelman et al. [45] for the operation of a central cooling plant in a district cooling system. For any FSM algorithm, the representation of the different states and the logical conditions is achieved with the aid of a state graph.

Fig. 5 shows a state graph for the heating mode controller in a DSS and the controller implementation is shown on the right side. The initial OFF state of the heating mode is denoted by the double square. The transition *T1* from OFF to ON state is triggered when $\dot{Q}_h > 0$ and a subsequent heating signal y with an integer value of 0 or 1 activates the heating circulation pump. A delay time forces the heating mode to remain active for 10 min before the transition to the OFF state to avoid short-cycling between the states.

A similar principle with additional states is seen in the cooling mode controller presented in Fig. 6. Unlike the single heating equipment that provides all required heating demands, cooling can be provided either directly by the free-cooling heat exchanger (Free Cooling mode), by fully using a mechanical chiller (Full Mechanical Cooling mode), or by a combination of both (Partial Mechanical Cooling mode). The state graph on the top of Fig. 6 describes the conditions that determine the transition between the states. The initial OFF state is also denoted here by the double square shown in the Modelica diagram. The reader is reminded that cooling demands are denoted by a negative sign, hence cooling is activated when $\dot{Q}_c < 0$. At a particular point in time when cooling is required, the transition between the different states is mainly determined based on the temperature of the district warm pipe $T_{dis,w}$ and the return temperature from the building cooling loop $T_{ret,c}$. When the condition $T_{dis,w} < T_{ret,c}$ holds, the transition *T2* triggers and the FC mode is activated. If the required cooling demand is larger than the capacity of the free-cooling heat exchanger $\dot{Q}_{hx} > \dot{Q}_c$, the transition *T4* activates the PMC state where the mechanical chiller covers the additional cooling demand. In case the temperature of the district warm pipe is no longer suitable for direct supply, the transition *T6* activates the FMC mode where cooling is provided solely by the mechanical chiller. The cooling control signal determines which circulation pump should be activated according to the arrangement of the cooling equipment shown previously in Fig. 2.

2.3.2. Control of the balancing unit

The balancing unit is controlled based on the dominant demand type across the network. At times of dominant cooling demands, the BU rejects the excess heat from the network. This is achieved by the cooling tower and the reversible ASHP which provide the required cooling according to the following control sequence. First, the operation of the cooling tower is determined by the controller shown in Fig. 7 when the following two conditions hold:

$$T_{air} < T_{dis,c} \quad \text{and} \tag{23}$$

$$T_{set,c} < T_{dis,c} + \frac{\text{bandwidth}}{2} \tag{24}$$

where T_{air} is the ambient air temperature, $T_{dis,c}$ is the temperature of the cold district pipe, $T_{set,c}$ is the network cooling setpoint, and the bandwidth makes the reference temperature passes over a certain predefined value (typically 1 °C) to induce a lag effect. The cooling tower is then activated and the output signal y shown in Fig. 7 controls the opening of the valve placed at the inlet of the cooling tower. Second, if at any point in time the capacity of the cooling tower is not sufficient to provide the required cooling power, the reversible ASHP is activated in a cooling mode such that:

$$T_{evap,lea} = T_{set,c} \tag{25}$$

where $T_{evap,lea}$ is the evaporator leaving temperature.

In the other situation when heating demands dominate, the reversible ASHP is activated in a heating mode to maintain the temperature of the district warm pipe such that:

$$T_{cond,lea} = T_{set,h} \tag{26}$$

where $T_{cond,lea}$ is the condenser leaving temperature and $T_{set,h}$ is the network heating setpoint.

2.4. Case study

The previously presented models for thermo-fluid systems and control logics have been used to assemble an entire district system. Fig. 8 shows a Modelica diagram view of the district system used in this study which is located in south Sweden. The buildings were previously connected to a traditional district heating and cooling network with a four-pipe network topology. Initial work to retrofit the energy system in the presented nine buildings to a 5GDHC network began in 2018 and the system is currently going through continuous expansion. The spaces in the buildings have different uses, including open offices, conference rooms, research labs, and sports halls. Overall, the facility

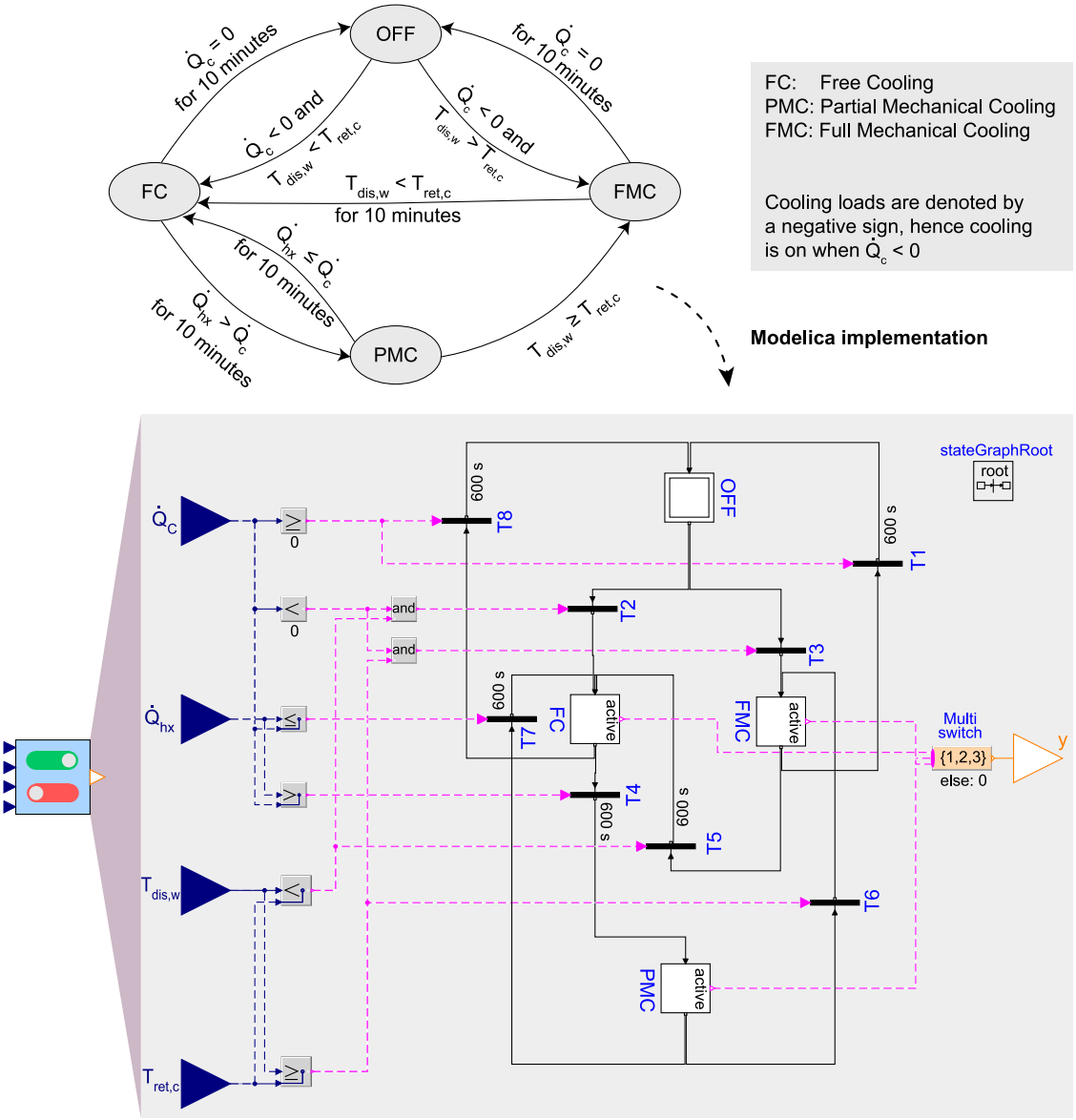

Fig. 6. State graph for the cooling mode controller (top) and equivalent Modelica implementation (bottom).

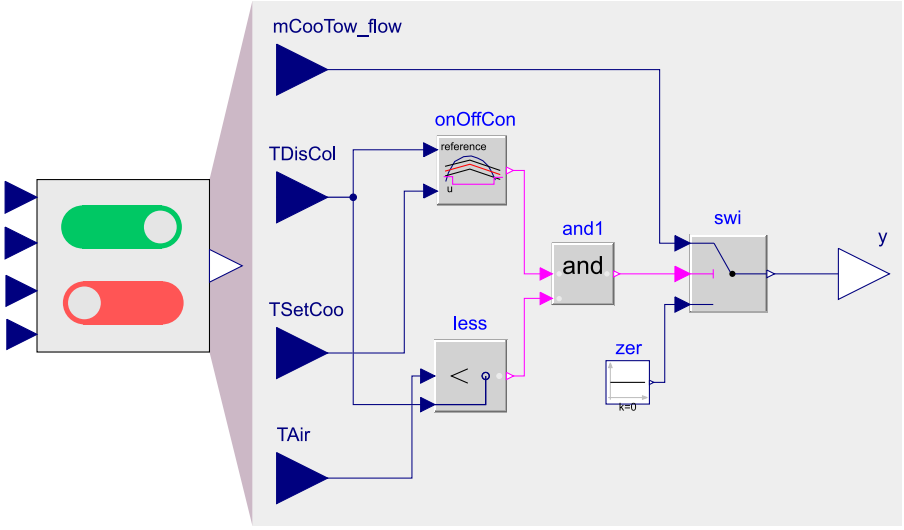

Fig. 7. Cooling tower controller.

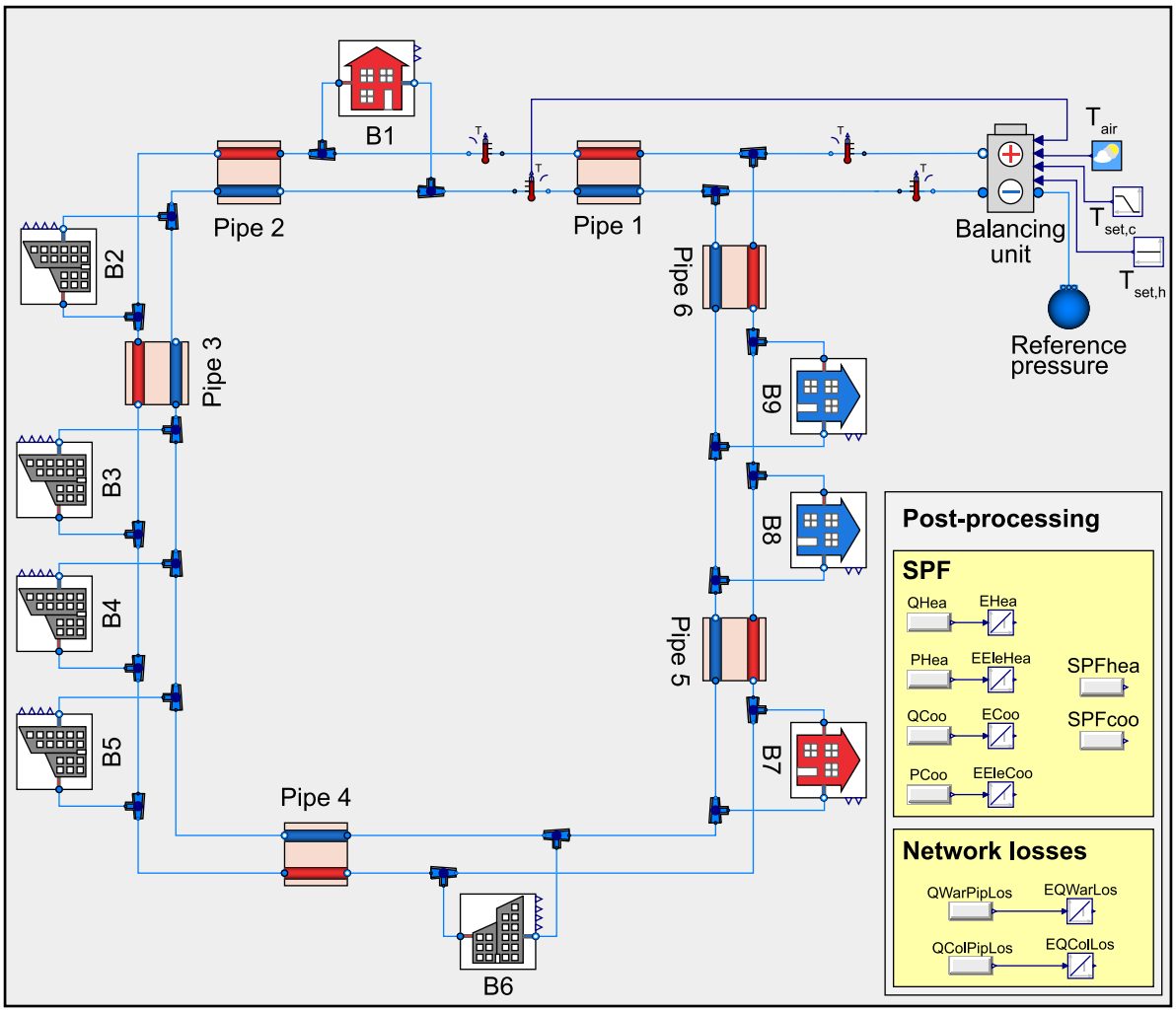

Fig. 8. Modelica diagram view of the studied district system showing the ring network topology, the nine connected buildings, and the balancing unit. The different pipe models indicate changes in the pipe size.

has simultaneous requirements for heating and cooling throughout the year.

All presented icons in Fig. 8 encapsulate the components which represent the model and exchange its variables with the connected models. For instance, the BU requires the following four variables to be prescribed: the temperature of the cold district pipe, the temperature of the ambient air, and the heating and cooling setpoints. The cold pipe temperature variable was obtained based on the feedback from the sensor located on the left side of Pipe 1 to break algebraic loops. The different pipe models indicate changes in the pipe size.

The model for the studied district system takes as inputs annual hourly measured data for buildings' heating and cooling demands and supply temperatures. Component models are parametrised based on actual design values and engineering assumptions. The tables in Appendix A provide an overview of the parameter values used in the models for decentralised substations, distribution pipes, and the balancing unit.

The district system was simulated on a desktop computer with 12 physical cores and 24 logical processors with a maximum speed of 3.50 GHz (AMD Ryzen Threadripper 2920X) and 32 GB of RAM running under Windows 10 Pro 64 bit. Dymola version 2022 [46] was used as the Modelica simulation environment since it offers a user-friendly interface for model development and post-processing. The CVODE integration algorithm was selected due to its efficiency in simulating thermo-fluid systems [47]. Simulations were performed for one year with one hour interval and tolerance of 1×10^{-6}.

2.5. Model probabilistic validation

Model probabilistic validation is used to study the impact of uncertainty on the model error since both measured data and model output have uncertainties [48]. Instead of directly determining mismatches between modelled and measured quantities, model probabilistic validation aims at establishing a relationship between error and probability. For this purpose, the cumulative distribution function (CDF) has been used to establish such relationship by following the steps shown in Fig. 9. The CDF is a continuous function bounded between 0 and 1 and provides the probability that a continuous random variable is less than or equal to a certain value. In this context, the CDF gives the probability that the absolute error Z between modelled and measured heat flow rate is less than or equal to an error benchmark level. The error Z is calculated as:

$$Z = \left| \frac{\dot{Q}_{mod} - \dot{Q}_{mea}}{\dot{Q}_{mea}} \right| \cdot 100 \tag{27}$$

where $\dot{Q}_{mod}$ and $\dot{Q}_{mea}$ are respectively the modelled and measured heat flow rates.

The first estimation of a reasonable error benchmark level can be equal to the maximum permissible error (MPE) of the thermal energy meter. The MPE of thermal energy meters is quantified in accordance with Standard SS-EN 1434-1 [49] and the sensor characteristics which are provided in Table B.1 in Appendix B. Evaluating the probability at

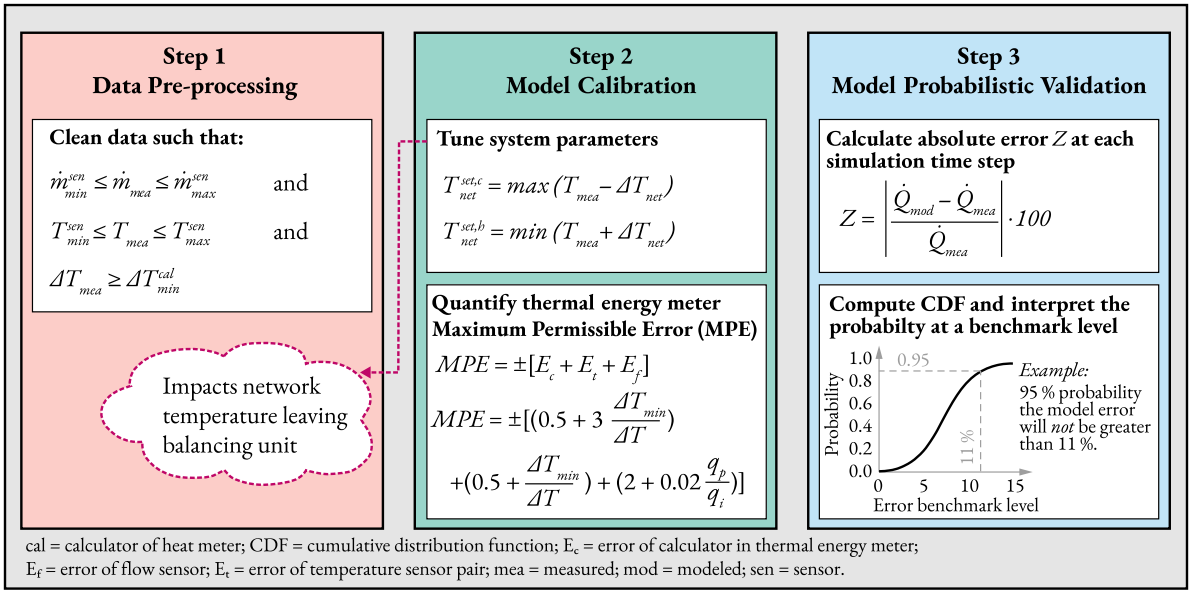

Fig. 9. Steps for performing model probabilistic validation.

different error benchmark levels is also useful to account, when possible, for other sources of uncertainties and to analyse the distribution of the error.

The model is validated using one-year data of heat flow rate from thermal energy meters located at the district side in each DSS. The heat flow rate is derived from measured entering and leaving temperatures as well as the measured mass flow rate. If the model calculates the heat flow rate with high confidence, an evaluation of the system performance can be made since the heat flow rate represents the actual exchanged heat between the DSS and the district system. In the first step shown in Fig. 9, data were pre-processed to exclude unrepresentative and faulty measurements. Depending on the characteristics of the thermal energy meter, faulty data were identified. For instance, data points with values that fall outside the range of the flow and temperature sensors were not considered. Moreover, data points with negative temperature differences yielded zero mass flow and zero heat flow rate. The second step involved determining a set of candidate parameters that can be used for model calibration. Because the calculation of the heat flow rate depends on the inlet and outlet temperatures, calibrating the network heating and cooling setpoints would directly impact the temperature in each DSS. Finally, the absolute error was calculated for each timestep and the probability of the model error was computed.

2.6. Performance indicators

The heating and cooling seasonal performance factor (SPF) are used as performance indicators. The SPF for all DSS is described according to the following boundaries:

$$SPF_{DSS} = \sum_{1}^{n} \sum_{t=o}^{8760} \frac{\dot{Q}}{P_{comp} + P_{pum,loa} + P_{pum1,dis} + P_{pum2,dis}} \tag{28}$$

where n is the number of buildings, t is the simulation time in hours, $\dot{Q}$ is the delivered thermal power, P_{comp} is the compressor electric power of the heat pump or the chiller, $P_{pum,loa}$ is the electric power of the circulation pump at the building load side, $P_{pum1,dis}$ and $P_{pum2,dis}$ are the electric power of the two circulation pumps located on the district side. Fig. 2 should be consulted to point out the location of these circulation pumps.

As for the BU, the heating and cooling SPF are calculated as:

$$SPF_{BU} = \sum_{t=o}^{8760} \frac{\dot{Q}}{P_{comp} + P_{fan}} \tag{29}$$

where P_{comp} and P_{fan} are the respective compressor and fan electric power of the reversible ASHP.

The SPF for the entire district system is defined as:

$$SPF_{system} = \sum_{t=o}^{8760} \frac{\dot{Q}_{DSS} + \dot{Q}_{BU}}{P_{DSS} + P_{BU}} \tag{30}$$

where $\dot{Q}_{DSS}$ is the total delivered thermal power by all DSS, $\dot{Q}_{BU}$ is the delivered power by the BU, P_{DSS} and P_{BU} are respectively the electric power used in the DSS and the BU.

2.7. Model simplifications and limitations

The presented models are subject to several simplifications and limitations that may influence the interpretation of the results. Firstly, the building demands and the supply from the BU are provided only by the component models presented in the previous sections. Auxiliary energy systems such as conventional DH that cover peak demands are therefore not considered in the analyses to limit the performance evaluation to the components that are typically included in a 5GDHC network. Secondly, models for heat pumps and chillers have unlimited capacity and deliver thermal power based on the required demand. This makes it easier to model DSS with multiple heat pumps or multiple chillers by aggregating the demands into individual components. Additionally, we limited model validation to the measured heat flow rate at the district source side since it would suffice for the validation of decentralised heat pumps and chillers according to the definition of the Carnot cycle. Moreover, the calculations of heat losses in the uninsulated pipes are for steady-state operation with no heat storage in the pipe wall or the soil. The temperature surrounding the pipes is assumed to be uniform. Finally, the heat carrying fluid in the district and building loops is incompressible water with constant properties.

3. Results

This section presents simulation results of the district system for aspects related to simulation performance, network supply–demand structure, network temperature and heat losses, and the overall system energy balance.

Table 1
Model statistics for a 5GDHC system comprising nine buildings.

Model statistic	Value
Number of components	5126
Number of equations	23 544
Number of parameters	29 028
CPU time for annual simulation [min]	4.56

Table 2
Probability of model error in calculating annual hourly heat flow rate at different locations and for different error benchmark levels.

Location of district supply thermal energy meter	Probability of model error ≤ Benchmark level (BL)		
	9% BL	14% BL	19% BL
Building 1 heating	0.424	0.918	0.945
Building 2 heating	0.957	0.971	0.978
Building 2 cooling	0.062	0.313	0.591
Building 3 heating	0.824	0.928	0.960
Building 3 cooling	0.950	0.968	0.971
Building 4 heating	0.900	0.983	0.993
Building 4 cooling	0.959	0.977	0.992
Building 5 heating	0.481	0.590	0.676
Building 5 cooling	0.971	0.991	0.995
Building 6 heating	0.947	0.967	0.976
Building 6 cooling	0.975	0.975	0.977
Building 7 heating	0.971	0.976	0.980
Building 8 cooling	0.896	0.993	0.999
Building 9 cooling	0.956	0.987	0.995

3.1. Model and simulation performance

Information about model statistics and the probability of model error are provided in Tables 1 and 2, respectively. The complexity of the model is directly associated with the required computational efforts to perform simulations. The results show that simulating the entire district system for a period of one year took less than five minutes. The short simulation time highlights the benefits of using Modelica for further research on district energy technologies. The model probabilistic validation shown in Table 2 presents the probability of model error at different error benchmark levels. A benchmark level of 9% corresponds to the Maximum Permissible Error (MPE) of the thermal energy meter which was quantified according to the formulas shown in Fig. 9. The two additional benchmark levels enable gaining greater insights into the probability of model error if more sources of uncertainty are considered. What stands out in the table is the high accuracy of modelled heat flow rates at several substations. Exceptions were found at three locations: *Building 1 heating*, *Building 2 cooling*, and *Building 5 heating*. The substations in these three locations have more than one heat pump or more than one chiller that are connected in series and, hence, the measured heat flow rate was influenced by the performance of each individual heat pump/chiller. Since the model for DSS includes only a single heat pump and a single chiller, this limitation could explain the difference between the modelled and measured heat flow rates in these three substations. Taken all together, comparing the probability of model error between the different benchmark levels reveals that the model has a probability of at least 95% where the error is less than 14% for most of the measurement locations. These results suggest that the model is in good agreement with the measurements and further analyses on the system performance can be carried out.

3.2. Breakdown of system supply–demand structure

Fig. 10 presents a breakdown of the simulated district supply–demand structure at different system levels. The ambient air temperature and the modelled soil temperature at the pipe burial depth are presented in Fig. 10(a). The air temperature affects the system control, e.g., the operation of the cooling tower, while the soil temperature impacts the heat losses (or gains) in the distribution pipes. Looking at Fig. 10(b), the illustrated total network demands show that the district system has a simultaneous requirement for heating and cooling throughout the year, with peak power for heating and cooling of about 1 MW. In Fig. 10(c), the total network mass flow is presented and can be interpreted as the total flow entering or leaving the BU in the direction towards or from the connected buildings. For instance, a negative mass flow would indicate a flow direction from the network to the BU. In other words, the dominant network cooling demands can lead to excess heat that flows from the network to the BU where the latter rejects the excess heat by the cooling tower and/or the reversible ASHP. On the other hand, a positive mass flow direction would denote a flow direction from the balancing unit towards the network. This situation can be realised when the network has dominant heating demands and the reversible ASHP injects heat into the network. Fig. 10(d) complements the system supply–demand structure where heating and cooling powers provided by the BU are presented. A comparison between the power provided by the cooling tower and the ASHP shows that the former can cover small portions of the required cooling power. This, in turn, would suggest that most of the cooling provided by the BU is achieved by compressors. The simulation results also show that no cooling is provided by the BU during the period from early November to mid-May. This implies that although the connected buildings have cooling demands, the network temperature remains below the cooling setpoint and therefore no network cooling is needed. A detailed analysis of the network temperature is covered in the following section.

3.3. Network temperature and heat losses/gains

In Fig. 11, the simulated annual hourly network temperature and network heat losses are presented. The network temperature shown in Fig. 11(a) is maintained between prescribed heating and cooling setpoints. The presented temperatures correspond to the temperature of the heat carrying fluid in the BU. As such, the BU maintains a constant warm fluid temperature at a setpoint of 18 °C during winter between November and April when network heating demands dominate. The effect of the network heat losses/gains on the warm fluid temperature during winter cannot be seen since the presented temperature corresponds to the fluid leaving the BU before distribution losses take effect. In contrast, the effect of the network heat losses/gains on the cold pipe temperature in the same winter period can be noticed since the fluid has already travelled along the pipes before entering the balancing unit. The calibrated cooling setpoint varies between the two summer periods. A cooling setpoint of 20 °C is used in the first summer period in August 2020, while a setpoint of 28 °C is used in July 2021. During spring and autumn, the fluid temperature changes more frequently as these are the periods where the dominant demand type changes within short intervals. As a consequence, the mass flow in the network reverses its direction depending on whether the balancing unit is injecting or rejecting heat, as Fig. 10(c) also shows. Although the network is designed for a 10 K temperature difference, the results suggest that such temperature difference is not always maintained due to the impact of network losses/gains on the fluid temperature.

Fig. 11(b) shows the network heat losses in all distribution pipes where a negative sign indicates heat gains. To obtain more clarity about the network losses/gains, the reader is advised to refer to the soil temperature presented earlier in Fig. 10(a) as it forms the boundary condition of the distribution pipes. Looking at the heat losses in cold pipes, one can see that the cold pipes are gaining heat most of the year even in winter months when the soil temperature is lower than the cold fluid temperature. This is primarily attributed to the anti-symmetrical component of the heat losses, i.e., the interaction between the two pipes due to the close distance between the warm and cold pipes at just 20 cm. From an annual perspective, the warm pipes have total heat losses to the ground of about 399 MWh, which corresponds to about 11% of the carried heat in all warm pipes. As for the cold pipes, the annual heat gains of 137 MWh constitute to about 7% of the carried heat in all cold pipes.

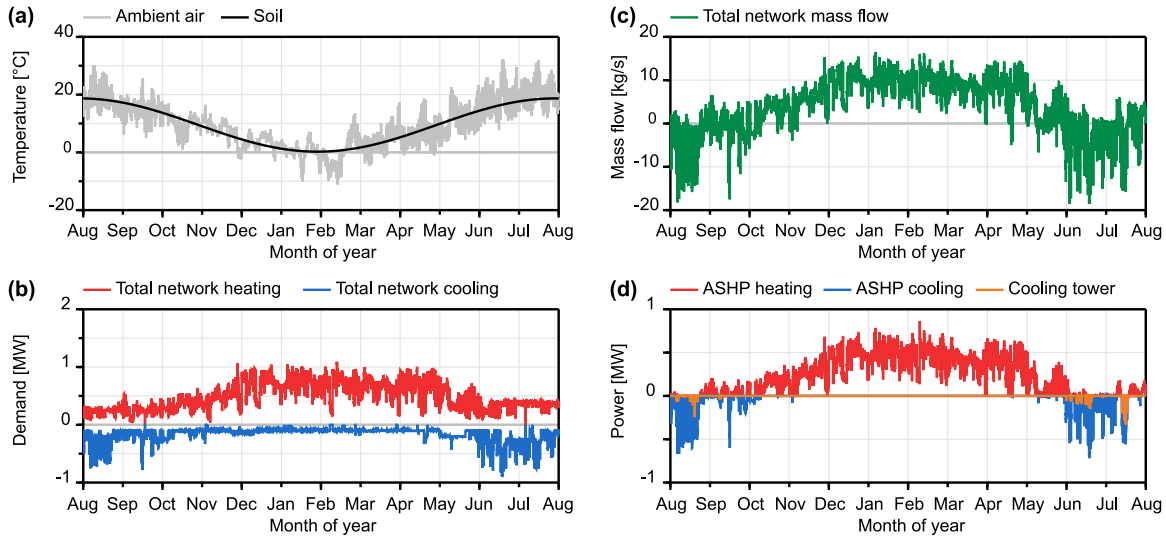

Fig. 10. Annual hourly simulation results of site climate conditions (a), total network heating and cooling demands (b), total network mass flow (c), and power provided by the balancing unit (d).

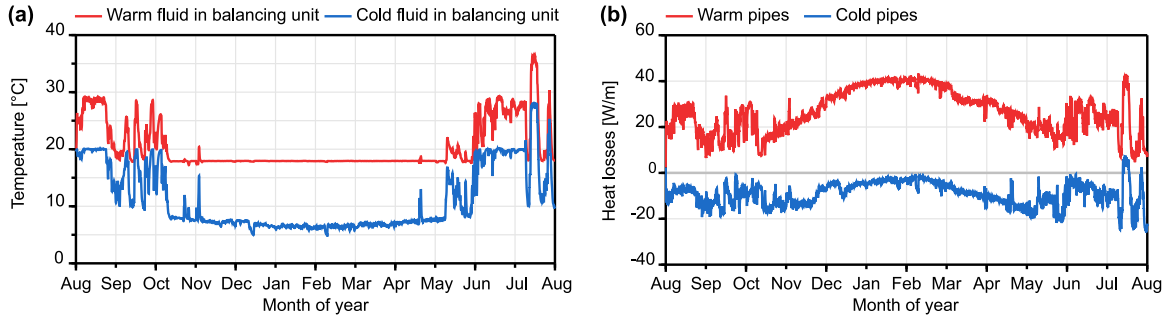

Fig. 11. Annual hourly network temperature (a) and network heat losses/gains (b) based on prescribed boundary conditions and network control setpoints. Negative heat flow rates indicate heat gains.

3.4. System energy balance and annual performance

To better understand the interactions between the buildings and the system components, Fig. 12 shows a Sankey diagram of the district system annual energy balance at different nodes. On the right-hand side, building heating and cooling demands are quantified according to measured data. Building demands are delivered by heat pumps and chillers located in each DSS. The amount of cooling provided by the free-cooling heat exchangers is not represented by an exclusive node in the diagram since it corresponds to only 0.3% of the annual delivered cooling. The total annual heating demands for all buildings are about 4.2 GWh, while the demands for cooling account for 1.2 GWh.

The interface between the DSS and the district supply side is realised at the cold side of each heat pump (HP) and alternatively at the warm side of each chiller (CH). The amount of energy extracted by the HP from the warm pipes is presented in the bars connecting the warm pipes and the HP. Likewise, CH extract energy from the cold pipes and reject waste heat to the warm pipes in an amount equivalent to the width of the connecting bars between the cold pipes and the CH. The annual network losses/gains are presented on the right-hand side of each pipe node. In this context, heat gains in the cold pipes may also be considered as losses since the desired temperature quality is not maintained. On that account, the total network losses in all distribution pipes constitute 10% of the annual carried heat. Compared to the latest statistics about the Swedish district heating system reported in 2020 [50], the modelled district network with uninsulated pipes can have 28% lower distribution losses than traditional networks with insulated pipes. Network heat losses/gains have an impact on the network temperature and, consequently, on the system's seasonal performance factor (SPF). The annual SPF at each DSS can be visually estimated from the Sankey diagram since the corresponding amount of electric energy is also provided.

The left-hand side of the warm and cold pipes represents the energy flows in the network as well as the balancing unit. Shared energy occurs both locally inside the DSS and globally between the connected buildings, it is represented in the Sankey diagram as a total amount for the whole year. Shred energy constitutes about 40% of the total carried heat in all distribution pipes and it can take one of two forms depending on the network demand type. The first form takes place when heating dominates and when the energy at the cold side of the heat pumps is utilised as a cold source for the chillers. Conversely, the second form of sharing energy happens when cooling dominates and when excess

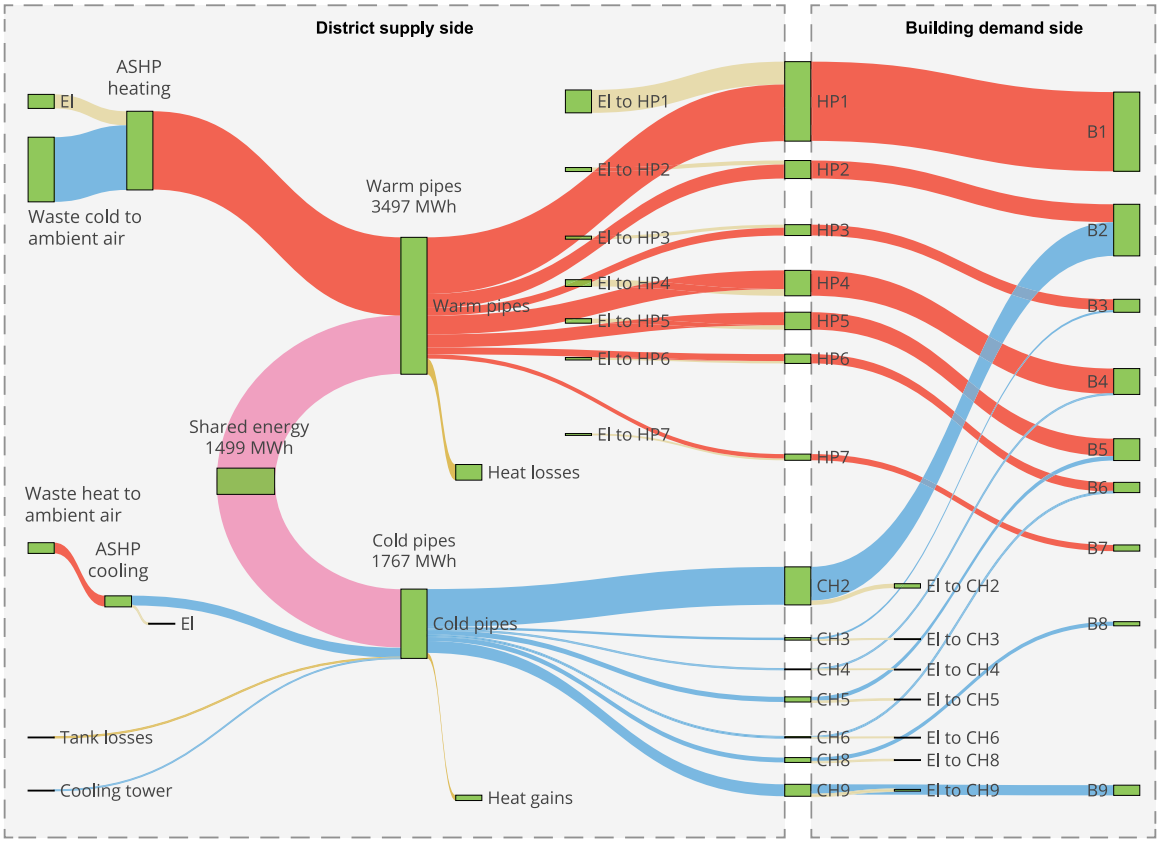

Fig. 12. Sankey diagram of the district system annual energy balance. The width of connecting bars is proportional to the amount of energy in unit MWh. Decentralised heat pumps (HP) and chillers (CH) represent the interface between the district supply and the building demand sides. The amount of shared energy is estimated to complement the system energy balance and it implies bidirectional energy flows between warm and cold pipes.

waste heat is rejected to the warm pipes. The excess waste heat acts as a hot source for the heat pumps and it is rejected outside the network when the temperature of the cold pipe reaches the cooling setpoint.

The mechanism for rejecting excess heat outside the network is achieved by the cooling tower and the reversible ASHP. About 2% of the rejected heat is handled by the cooling tower, while the rest is handled by the ASHP. The connection between tank losses and the cold pipes is established to represent the energy direction that flows out of the network. In the second mode of operation of the reversible ASHP, heat is injected into the network to maintain the temperature of the warm pipes according to the heating setpoint. Waste heat and waste cold from the ASHP to the ambient air are equivalent to 274 and 1651 MWh, respectively. These figures depend mainly on the performance of the ASHP.

Fig. 13 shows the annual heating and cooling SPF at different system levels. Overall, the system yielded good performance at all analysed levels. The highest performance was found in the BU due to the low temperature lifts required by the ASHP.

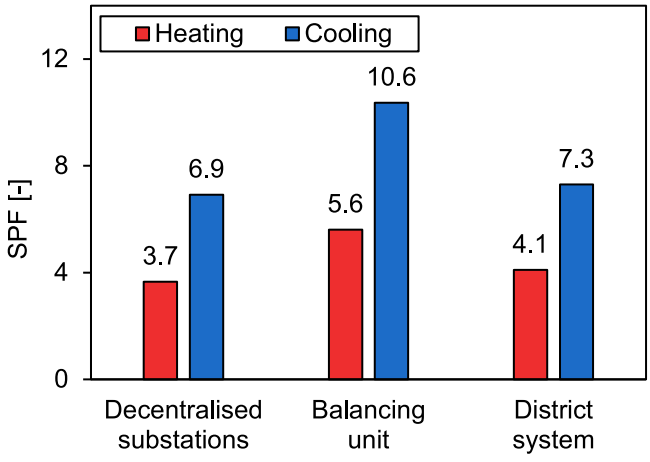

Fig. 13. Heating and cooling seasonal performance factors at different system levels.

4. Discussion

The study presented a simulation model for the design and analysis of 5GDHC systems with two-pipe network topology and bidirectional energy flows. Lessons learned during the design, operation, modelling, and simulation of the system are shared in this section. The main discussion points encompass the applicability of the simulation model in addition to a few practical recommendations for future wider implementation.

The findings in this study confirm the benefits of integrating district and heat pump technologies. To mention a few, district thermal networks are transformed into electricity-driven networks. Simulation

results showed that an electricity-driven 5GDHC system could reduce the purchased energy by 69% compared to a traditional four-pipe district heating and cooling system. Moreover, coupling the electricity and heat sectors adds more flexibility to the power grid by alleviating the problem of intermittent electricity production. As more electricity will be generated from renewable sources with intermittent production such as wind and solar [51], heat pumps can operate at full capacity when the electricity production is high to store the additional heat in the accumulator tank for later use.

The developed simulation model has several practical implications where it can be used at different implementation stages. In the planning stage of a new 5GDHC system, the model can be used to find promising building clusters that increase the potential for sharing energy between interconnected buildings. When such a cluster has been identified, several system design options can be evaluated, and an optimal design option can be selected. Defining appropriate parameter values and sizing system components are carried out during the design stage. In the final stage when the system is realised, the model can be used by the system owner for real-time system monitoring and operation to optimise daily to weekly system operation based on network temperature levels, electricity spot price, and amount of shared energy.

Possible practical recommendations for improving the system performance are listed herein. The results showed that extremely little cooling was provided by the free-cooling heat exchangers. We found two aspects that directly influenced this. Firstly, many of the connected buildings integrate room systems with low cooling return temperature than the temperature at the primary district side of the heat exchanger. This violates the condition for operating the free-cooling heating exchanger. Secondly, the network temperature setpoints are not primarily defined to maximise the utility of the free-cooling heat exchanger. It might be useful for future work to investigate the role of ground thermal storage and network setpoints on the potential to supply free cooling.

Wider implementation of 5GDHC systems should not be seen as replaceable of existing traditional DHC systems. Rather, a synergy can be established where 5GDHC systems can be built in newly built areas in the urban environment such that traditional DHC systems function as balancing units. In such configuration, the return pipe of the traditional DHC system is connected as a source for the 5GDHC system, which may also increase the capacity of existing traditional systems without increasing the flow. In addition, small-scale 5GDHC systems can increase the market share of district systems by connecting households in villages and small communities where access to traditional DHC systems is limited. In all cases, new business transactions need to be developed to support the sharing of energy between prosumers without neglecting non-technical factors such as alternative financing schemes, social acceptance, and national legislations.

5. Conclusions and future work

This study presented a simulation model for the design and analysis of district systems with simultaneous heating and cooling demands. The model enables simulating any number of buildings connected to a two-pipe network topology with bidirectional energy flows. Annual simulations performed on an existing Swedish district system with similar characteristics enabled gaining a deeper understanding of the mechanisms in which new advanced district systems may operate. Additionally, the simulations provided an in-depth analysis of important operational aspects related to shared energy flows between interconnected buildings, network heat losses (or gains), and system energy balance.

The model can be utilised in different use cases, including design optimisation of new systems, or for performance optimisation of existing systems. In the former use case, the model is used to evaluate the feasibility of different design options and system configurations. While in the latter the model can be used for real-time system monitoring and performance optimisation. For improved system performance, it is recommended to maximise the utility of free cooling by controlling the temperature of the cold pipeline to make it suitable for direct supply without local conditioning.

Extending the current model to include economic analysis would pave the way towards more research on flexibility by coupling thermal and power sectors. The economic analysis enables optimising the system heat production according to electricity spot price where additional heat can be produced and stored at times of low electricity price. Moreover, future research should focus on developing new business models for the prosumer concept considering alternative financing schemes, social acceptance, and national legislations.

CRediT authorship contribution statement

Marwan Abugabbara: Conceptualization (lead), Data curation, Investigation, Formal analysis, Methodology, Software, Validation, Visualization, Writing – original draft (lead), Writing – review & editing (supporting). **Saqib Javed:** Conceptualization (supporting), Project administration (supporting), Funding acquisition (equal), Supervision (lead), Writing – original draft (supporting), Writing – review & editing (lead). **Dennis Johansson:** Resources, Project administration (lead), Funding acquisition (equal), Supervision (supporting), Writing – original draft (supporting).

Declaration of competing interest

The authors declare that they have no known competing financial interests or personal relationships that could have appeared to influence the work reported in this paper.

Data availability

The authors do not have permission to share data.

Acknowledgements

The authors would like to acknowledge Jonas Lindhe who was at the time of conducting this research in a position at E.ON Sverige AB. Without his technical experience and engagement in discussions, this work would have been difficult to realise. The authors would also like to acknowledge Per Rosén from E.ON Sverige AB for the rewarding technical discussions and exchange of ideas that have had a positive impact on this work. All authors have read and agreed to the published version of the manuscript.

Funding organisations

This work was supported by the Swedish Energy Agency, project Ectogrid – A sustainable society by use and optimisation of shared local energy surplus [grant number 45952–1]; the European Regional Development Fund, project COOLGEOHEAT: Shallow geothermal energy – the green and effective heating and cooling grids of the future [grant number NYPS 20293146]; the Swedish Energy Agency, project Flexibility by implementation of heat pumps in thermal networks – Swedish participation in the IEA HPT annex [grant number 51525-1].

Appendix A. Design parameters

This appendix provides values for design parameters used in the DSS model (see Table A.1), pipe model (see Tables A.2 and A.3), and the balancing unit model (see Table A.4).

Pipe dimensions shown in Table A.3 are according to Standard SS-ISO 4427-2 [52] and provided for a standard dimension ratio equal to 17.

Table A.1
Design parameters used in the DSS model.

Parameter description	Symbol	Value	Unit
Temperature difference of heat pump/chiller condenser (outlet–inlet)	$\Delta T_{HP,cond}$	4[a]	K
Temperature difference of heat pump/chiller evaporator (outlet–inlet)	$\Delta T_{HP,evap}$	−4[a]	K
Temperature difference of district loop (warm–cold)	ΔT_{dis}	10[a]	K
Pressure difference over heat pump/chiller condenser and evaporator at nominal flow	$\Delta p_{cond/evap}$	30 000[b]	Pa
Carnot efficiency	η_{Carnot}	50[b]	%
Pump combined hydraulic and motor efficiencies	$\eta_{hyd/mot}$	49[b]	%

[a]Value based on system design and/or measurements.
[b]Value based on engineering experience.

Table A.2
Design parameters used in the distribution pipes model.

Parameter description	Symbol	Value	Unit
Burial depth to pipe upper surface	B	0.8[a]	m
Horizontal distance between pipe walls	A	0.2[a]	m
Thermal conductivity of soil	λ_{soil}	1.6[b]	W/m K
Thermal conductivity of pipe	λ_{pipe}	0.17[a]	W/m K

[a]Value based on system design and/or measurements.
[b]Value based on engineering experience.

Table A.3
Design parameters of different pipe sections.

Pipe section[c]	Nominal size	Wall thickness [mm]	Roughness [m][a]	Length [m][b]
Pipe 1	DN250	14.8	2.5×10^{-5}	150
Pipe 2	DN225	13.4	2.5×10^{-5}	200
Pipe 3	DN200	11.9	2.5×10^{-5}	500
Pipe 4	DN250	14.8	2.5×10^{-5}	210
Pipe 5	DN225	13.4	2.5×10^{-5}	150
Pipe 6	DN225	13.4	2.5×10^{-5}	500

[a]Value based on engineering experience.
[b]Value based on system design and/or measurements.
[c]The reader is advised to refer to Fig. 8 to locate each pipe section on the model diagram.

Table A.4
Design parameters used in the BU model.

Parameter description	Symbol	Value	Unit
Temperature difference at the water side of the reversible ASHP	ΔT_1	10[b]	K
Temperature difference at the air side of ASHP	ΔT_2	2[a]	K
Pressure difference over water side of ASHP at nominal flow	Δp_1	30 000[a]	Pa
Pressure difference over air side of ASHP at nominal flow	Δp_2	6000[a]	Pa
Carnot efficiency	η_{Carnot}	50[a]	%
Tank volume	V_{tank}	150[b]	m^3
Tank height	H_{tank}	15.6[b]	m
Tank insulation thickness	t_{ins}	40[b]	mm
Thermal conductivity of tank insulation material	λ_{ins}	0.036[b]	W/m K
Cooling tower approach temperature	ΔT_{APP}	2[a]	K

[a]Value based on engineering experience.
[b]Value based on system design and/or measurements.

Table B.1
Characteristics of thermal energy meters, flow sensors, and temperature sensors.

Connection size	Nominal flow rate q_p[m^3/h]	Minimum flow rate q_i [m^3/h]	Maximum flow rate q_s [m^3/h]	Temperature range [°C]	Minimum temperature difference ΔT_{min} [K]
DN65	25	0.25	50	5–130	3
DN80	40	0.40	80	5–130	3
DN100	60	0.60	120	5–130	3
DN150	150	1.50	300	5–130	3

Appendix B. Characteristics of thermal energy meters

See Table B.1

References

[1] Larsen MA, Petrović S, Radoszynski AM, McKenna R, Balyk O. Climate change impacts on trends and extremes in future heating and cooling demands over europe. Energy Build 2020;226:110397. http://dx.doi.org/10.1016/J.ENBUILD.2020.110397.

[2] United Nations. World urbanization prospects 2018: highlights. Tech. rep., 2018.

[3] The future of cooling. Tech. rep., Paris: IEA; 2018, URL https://www.iea.org/reports/the-future-of-cooling.

[4] European Commission. An EU strategy on heating and cooling: Com(2016) 51 final. 2016, URL https://eur-lex.europa.eu/legal-content/EN/TXT/?qid=1575551754568&uri=CELEX:52016DC0051.

[5] Frederiksen S, Werner S. District heating and cooling. Lund: Studentlitteratur AB; 2013.

[6] Mazhar AR, Liu S, Shukla A. A state of art review on the district heating systems. Renew Sustain Energy Rev 2018;96:420–39. http://dx.doi.org/10.1016/j.rser.2018.08.005.

[7] Zarin Pass R, Wetter M, Piette MA. A thermodynamic analysis of a novel bidirectional district heating and cooling network. Energy 2018;144:20–30. http://dx.doi.org/10.1016/j.energy.2017.11.122.

[8] Werner S. District heating and cooling in Sweden. Energy 2017;126:419–29. http://dx.doi.org/10.1016/j.energy.2017.03.052.

[9] Electricity supply, district heating and supply of natural gas 2019. final statistics. Tech. rep., Statistics Sweden; 2019, URL https://www.scb.se/publication/40414.

[10] Lund H, Werner S, Wiltshire R, Svendsen S, Thorsen JE, Hvelplund F, Mathiesen BV. 4Th generation district heating (4GDH): Integrating smart thermal grids into future sustainable energy systems. Energy 2014;68:1–11. http://dx.doi.org/10.1016/j.energy.2014.02.089.

[11] Werner S. International review of district heating and cooling. Energy 2017;137:617–31. http://dx.doi.org/10.1016/j.energy.2017.04.045.

[12] Pellegrini M, Bianchini A. The innovative concept of cold district heating networks: A literature review. Energies 2018;11(236). http://dx.doi.org/10.3390/en11010236.

[13] Østergaard PA, Werner S, Dyrelund A, Lund H, Arabkoohsar A, Sorknæs P, Gudmundsson O, Thorsen JE, Mathiesen BV. The four generations of district cooling - a categorization of the development in district cooling from origin to future prospect. Energy 2022;253:124098. http://dx.doi.org/10.1016/J.ENERGY.2022.124098.

[14] Lund H, Østergaard PA, Nielsen TB, Werner S, Thorsen JE, Gudmundsson O, Arabkoohsar A, Mathiesen BV. Perspectives on fourth and fifth generation district heating. Energy 2021;227:120520. http://dx.doi.org/10.1016/j.energy.2021.120520.

[15] Sulzer M, Werner S, Mennel S, Wetter M. Vocabulary for the fourth generation of district heating and cooling. Smart Energy 2021;1:100003. http://dx.doi.org/10.1016/J.SEGY.2021.100003.

[16] Calise F, Cappiello FL, Dentice d'Accadia M, Petrakopoulou F, Vicidomini M. A solar-driven 5th generation district heating and cooling network with ground-source heat pumps: a thermo-economic analysis. Sustainable Cities Soc 2022;76:103438. http://dx.doi.org/10.1016/J.SCS.2021.103438.

[17] Lindhe J, Javed S, Johansson D, Bagge H. A review of the current status and development of 5GDHC and characterization of a novel shared energy system. Sci Technol Built Environ 2022;1–15. http://dx.doi.org/10.1080/23744731.2022.2057111.

[18] Revesz A, Jones P, Dunham C, Davies G, Marques C, Matabuena R, Scott J, Maidment G. Developing novel 5th generation district energy networks. Energy 2020;201:117389. http://dx.doi.org/10.1016/j.energy.2020.117389.

[19] Revesz A, Dunham C, Jones P, Bond C, Fenner R, Moody S, Nijjhar R, Marques C, Maidment G. A holistic design approach for 5th generation smart local energy systems: Project greenSCIES. Energy 2022;242:122885. http://dx.doi.org/10.1016/J.ENERGY.2021.122885.

[20] Arabkoohsar A, Alsagri AS. Thermodynamic analysis of ultralow-temperature district heating system with shared power heat pumps and triple-pipes. Energy 2020;194:116918. http://dx.doi.org/10.1016/j.energy.2020.116918.

[21] Quirosa G, Torres M, Soltero VM, Chacartegui R. Energetic and economic analysis of decoupled strategy for heating and cooling production with CO2 booster heat pumps for ultra-low temperature district network. J Build Eng 2022;45:103538. http://dx.doi.org/10.1016/J.JOBE.2021.103538.

[22] Reiners T, Gross M, Altieri L, Wagner H-J, Bertsch V. Heat pump efficiency in fifth generation ultra-low temperature district heating networks using a wastewater heat source. Energy 2021;236:121318. http://dx.doi.org/10.1016/J.ENERGY.2021.121318.

[23] Bünning F, Wetter M, Fuchs M, Müller D. Bidirectional low temperature district energy systems with agent-based control: Performance comparison and operation optimization. Appl Energy 2018;209(2017):502–15. http://dx.doi.org/10.1016/j.apenergy.2017.10.072.

[24] Wirtz M, Kivilip L, Remmen P, Müller D. Quantifying demand balancing in bidirectional low temperature networks. Energy Build 2020;224:110245. http://dx.doi.org/10.1016/j.enbuild.2020.110245.

[25] Buffa S, Cozzini M, D'Antoni M, Baratieri M, Fedrizzi R. 5Th generation district heating and cooling systems: A review of existing cases in Europe. Renew Sustain Energy Rev 2019;104(2018):504–22. http://dx.doi.org/10.1016/j.rser.2018.12.059.

[26] Wirtz M, Kivilip L, Remmen P, Müller D. 5Th generation district heating: A novel design approach based on mathematical optimization. Appl Energy 2020;260:114158. http://dx.doi.org/10.1016/j.apenergy.2019.114158.

[27] von Rhein J, Henze GP, Long N, Fu Y. Development of a topology analysis tool for fifth-generation district heating and cooling networks. Energy Convers Manage 2019;196:705–16. http://dx.doi.org/10.1016/j.enconman.2019.05.066.

[28] Modelica Association. [Modelica association]. 2021, URL https://modelica.org/.

[29] Sommer T, Sulzer M, Wetter M, Sotnikov A, Mennel S, Stettler C. The reservoir network: A new network topology for district heating and cooling. Energy 2020;199:117418. http://dx.doi.org/10.1016/J.ENERGY.2020.117418.

[30] Millar MA, Yu Z, Burnside N, Jones G, Elrick B. Identification of key performance indicators and complimentary load profiles for 5th generation district energy networks. Appl Energy 2021;291:116672. http://dx.doi.org/10.1016/j.apenergy.2021.116672.

[31] Meibodi SS, Loveridge F. The future role of energy geostructures in fifth generation district heating and cooling networks. Energy 2021;122481. http://dx.doi.org/10.1016/J.ENERGY.2021.122481.

[32] Wetter M, Van Treeck C. New generation computational tools for building and community energy systems annex 60 final report. 2017, http://dx.doi.org/10.4103/0973-1229.86137, no. September.

[33] Abugabbara M, Javed S, Bagge H, Johansson D. Bibliographic analysis of the recent advancements in modeling and co-simulating the fifth-generation district heating and cooling systems. 2020, http://dx.doi.org/10.1016/j.enbuild.2020.110260.

[34] Wetter M. Modelica-based modelling and simulation to support research and development in building energy and control systems. J Build Perform Simul 2009;2(2):143–61. http://dx.doi.org/10.1080/19401490902818259.

[35] Wetter M, Zuo W, Nouidui TS, Pang X. Modelica buildings library. J Build Perform Simul 2014;7(4):253–70. http://dx.doi.org/10.1080/19401493.2013.765506.

[36] Müller D, Remmen P, Constantin A, Lauster M, Fuchs M. AixLib - an open-source modelica library within the IEA-EBC annex60 framework. In: BauSIM. 2016.

[37] Baetens R, De Coninck R, Jorissen F, Picard D, Helsen L, Saelens D. Openideas - an open framework for integrated district energy simulations. In: 14th international conference of IBPSA - building simulation 2015, BS 2015, conference proceedings. 2015, p. 347–54.

[38] SS-EN 13941-1:2019 district heating pipes – design and installation of thermal insulated bonded single and twin pipe systems for directly buried hot water networks – part 1, design. Tech. rep., S. Institutet För Standarder; 2021.

[39] Wallentén P. Steady-state heat loss from insulated pipes (Ph.D. thesis), Division of Building Physics, Lund University; 1991.

[40] van der Heijde B, Aertgeerts A, Helsen L. Modelling steady-state thermal behaviour of double thermal network pipes. Int J Therm Sci 2017;117:316–27. http://dx.doi.org/10.1016/j.ijthermalsci.2017.03.026.

[41] ASHRAE. District heating guide. Atlanta: American Society of Heating, Refrigerating and Air-Conditioning Engineers, Inc.; 2013.

[42] Modelica. Wallfriction documentation. 2020, URL https://doc.modelica.org/Modelica4.0.0/Resources/helpDymola/Modelica_Fluid_UsersGuide_ComponentDefinition.html#Modelica.Fluid.UsersGuide.ComponentDefinition.WallFriction

[43] Goyal S. Advanced contols for intelligent buildings: a holistic approach for successful businesses. 1st ed.. CRC Press; 2021.
[44] Fu Y, Zuo W, Wetter M, VanGilder JW, Han X, Plamondon D. Equation-based object-oriented modeling and simulation for data center cooling: A case study. Energy Build 2019;186:108–25. http://dx.doi.org/10.1016/j.enbuild.2019.01.018.
[45] Hinkelman K, Wang J, Fan C, Zuo W, Gautier A, Wetter M, Long N. A case study on condenser water supply temperature optimization with a district cooling plant. In: Proceedings of 14th modelica conference 2021, linköping, Sweden, september 20-24, (2021). 2021, p. 587–95. http://dx.doi.org/10.3384/ecp21181587.
[46] Dassault Systèmes. DYMOLA systems engineering. 2021, URL https://www.3ds.com/products-services/catia/products/dymola/.
[47] Hinkelman K, Wang J, Zuo W, Gautier A, Wetter M, Fan C, Long N. Modelica-based modeling and simulation of district cooling systems: A case study. Appl Energy 2022;311:118654. http://dx.doi.org/10.1016/J.APENERGY.2022.118654.
[48] Roy CJ, Oberkampf WL. A comprehensive framework for verification, validation, and uncertainty quantification in scientific computing. Comput Methods Appl Mech Engrg 2011;200:2131–44. http://dx.doi.org/10.1016/J.CMA.2011.03.016.
[49] SS-EN 1434-1. Thermal energy meters– part 1: general requirements. Tech. rep., SVENSK STANDARD; 2018.
[50] Statistics Sweden. District heating. 2022, URL https://www.scb.se/en/finding-statistics/statistics-by-subject-area/energy/energy-supply-and-use/annual-energy-statistics-electricity-gas-and-district-heating/pong/tables-and-graphs/district-heating/.
[51] Government Offices of Sweden. Agreement on Swedish energy policy. 2016, URL https://www.government.se/articles/2016/06/agreement-on-swedish-energy-policy/.
[52] SS-ISO 4427-2. Plastics piping systems for water supply, and for drainage and sewerage under pressure – polyethylene (pe) – part 2: pipes. Tech. rep., 2019.